

# Capacitance Value Control for Metamaterial Reflectarray using Multi-layer Mushroom Structure with Parasitic Patches

Tamami Maruyama, Tatsuo Furuno, Yasuhiro Oda, Jiyun Shen, and Tomoyuki Ohya

NTT DOCOMO, Inc., 3-5 Hikari-no-oka, Yokosuka, Kanagawa 239-8536 Japan  
 maruyamatam@nttdocomo.co.jp, furuno@nttdocomo.com, oday@nttdocomo.co.jp,  
 shink@nttdocomo.co.jp, ooyat@nttdocomo.co.jp

**Abstract** — A mushroom-structure reflectarray can be designed by setting the values of inductance  $L$  and capacitance  $C$  based on  $LC$  resonant circuit theory. Since the capacitance value is determined by the gap size of mushroom patches and the range of the gap size is limited by the manufacturing process, it is difficult to adjust the capacitance value to achieve the desired reflection phase for the reflectarray design. To address this issue, this paper proposes introducing multi-layer parasitic patches on the mushroom structure and controlling the capacitance values using the number of parasitic layers based on the parallel resonant circuit theory. This paper also proposes a novel design method for mushroom reflectarrays when the incident electric field and beam control direction of the scattered waves are set parallel by focusing on the capacitance value. We measure reflected and scattered waves in an anechoic chamber. The measurement results of the direction of the reflected wave are shown compared to the results of the theoretical and simulation analyses.

**Index Terms** — Artificial magnetic conductors (AMC), high impedance surface (HIS),  $LC$  resonant circuit model, metamaterial, multi-layer mushroom, mushroom-like structure, reflectarray.

## I. INTRODUCTION

Recently, the study and standardization of very high-speed (beyond 2 Gbps) wireless communication systems [1] have progressed. By using high frequency radio waves, we can allocate a sufficient bandwidth to achieve high data transmission rates in these systems. The coverage area however, becomes smaller when using a high frequency because the propagation loss increases

due to diffraction, and this leads to difficulty in using high frequencies in mobile communications. In order to address this issue, we proposed using reflectarrays placed on the top of buildings to eliminate blind zones in the valleys between buildings by controlling the direction of the scattered waves using the reflectarrays [2-6]. One of these reflectarrays is constructed using an approximate half wavelength cross dipole element array and an approximate one wavelength loop array for the ground plane that can simultaneously achieve dual polarization and frequency selective characteristics [2,4,6]. On the other hand, there are some reports of metamaterial reflectarrays that employ a mushroom structure, the elements for which are very short compared to the wavelength [3,7-10]. The metamaterial structure reflectarray is regarded as an artificial material that can control reflected waves in directions other than a mirror image, and the reflection phase can be calculated using a parallel resonant circuit model with inductance  $L$  and capacitance  $C$  [7]. The reflection phase is equal to zero at the  $LC$  resonant frequency and the reflection phase varies from  $+\pi$  to  $-\pi$  as the frequency changes. The resonant frequency can be controlled by changing the values of  $L$  and  $C$ , and there are typically three control methods [3,7-10]. The first method employs varactor diodes and changes in the voltage [7], the second method changes the via position of the mushroom structure [10], and the third involves changing the patch length of the mushroom structure to achieve a difference in capacitance [3,8,9]. There are mainly two problems with these conventional methods [3,7-10] when we focus on controlling the capacitance value in the design of mushroom reflectarrays based on the  $LC$  resonant frequency.

The first problem is the limitation caused by the manufacturing process. Although, it is necessary to achieve a reflection phase range from  $+\pi$  to  $-\pi$  at the desired frequency in the design of a reflectarray, it is difficult to achieve this. For example in the case of the third method [8, 9], it is necessary to close the distance between the mushroom patches to achieve a high capacitance; however, the degree to which the interval between the patches can be reduced is limited by the manufacturing process.

The other problem is the design method. In the conventional reflectarray design method [12, 8, 9], the element length is considered to determine the resonant frequency. However, in the mushroom reflectarray design, the resonant frequency is considered to be the  $LC$  resonant frequency, which is determined by  $L$  and  $C$ . Since the capacitance value depends on the size of the gap between elements, the size of the gap is more important than the element length. Therefore, in designing when the incident electric field and beam control direction of the scattered waves are set parallel, it is difficult to adjust the capacitance value using the conventional design method.

To address these issues, this paper proposes a novel multi-layer mushroom reflectarray in which the structure is decided not by the size of the element but by the size of the gap between the elements. In order to adjust the capacitance value, we apply the circuit theory such that the  $n$ -parallel arranged capacitances generate  $n$ -times capacitance and set parasitic patch layers on the mushroom structure to form a parallel capacitance arrangement.

A multi-layered mushroom structure is used to increase the capacitance in order to achieve low frequency resonance [11]. However, the patch arrangement in [11] is different from that proposed in this paper. The performance of the proposed multi-layer mushroom reflectarray is shown by using the finite element method analysis, theoretical calculation based on parallel circuit theory, and measurement. For this purpose, we constructed systems to measure the reflection and transmission scattering waves in a chamber. The actual measurement results of the scattering pattern are shown compared with theoretical results using a radar equation and radar cross section (RCS) calculated using the high frequency structure simulator (HFSS). The pattern

configurations of both measurement and theoretical results are very similar and the difference of desired main beam direction at  $-70$  deg. is less than 3 dB.

A ‘‘homogenization model’’ was proposed recently for the analysis of a mushroom structure [15, 16, 17]. In this paper, we use both homogenization and  $LC$  resonant models for 1 layer mushroom. We show the homogenization model has advantage for accuracy. For the multi-layer mushroom calculation, we focus more on the qualitative behavior concerning parasitic patches for a mushroom structure than the quantitative accuracy, and choose Sievenpiper’s model [13].

## II. EFFECT AND ANALYSIS OF PARALLEL SET CAPACITANCES

The  $LC$  resonant frequency of the mushroom structure can be changed as shown in (1) using variations in capacitance ‘‘ $C$ ’’ and inductance ‘‘ $L$ ’’ as reported in [13]. In formula (1), ‘‘ $\omega$ ’’ is the angular frequency.

$$\omega = 2\pi f = 1/\sqrt{LC}. \quad (1)$$

Table 1: Design parameters

Parameter	Symbol
Element space of mushroom structure for $x$ axis direction	$\Delta x$
Element space of mushroom structure for $y$ axis direction	$\Delta y$
Mushroom patch size for $x$ axis direction	$W_{mx}$
Mushroom patch size for $y$ axis direction	$W_{my}$
Parasitic patch size for $x$ axis direction	$W_{px}$
Parasitic patch size for $y$ axis direction	$W_{py}$
Gap size between mushroom patches: $\Delta y - W_{my}$	$g_y$
Gap size between parasitic patches: $\Delta y - W_{py}$	$g_{yp}$
Mushroom height	$t$
Interval between parasitic patches	$t_1, \dots, t_{n-1}$
Metallic ground layer	$L_0$
Mushroom patch layer	$L_1$
Parasitic patch layers	$L_2, \dots, L_n$
Dielectric substrate layers	$D_0, \dots, D_n$

This paper proposes a multi-layer mushroom structure for a reflectarray, which is shown in Fig. 1, that uses parasitic patches to obtain a wider variation in the capacitance value. Figure 1(a) shows a  $n$  layer mushroom structure consisting of a mushroom structure and  $n-1$  parasitic patch layers set on the mushroom structure. We use these parasitic patches to achieve  $n$  set parallel capacitance. A resonant circuit model and analysis model for the reflection phase calculation of the multi-layer mushroom structure are shown in Fig. 1(b) and 1(c), respectively. Table 1 gives the symbols and names of the parameters for the proposed structure. In terms of a non-parasitic layer mushroom structure, (2) - (5) are introduced based on a parallel resonant model as described in [13] using the parameters shown in Fig. 1 and

Table 1. Inductance  $L$  in Fig. 1 is approximated by the product of permeability and the mushroom thickness,  $t$ , shown in (2). The gap between patches is expressed as (3). Capacitance  $C$  is determined by the gap between the adjacent mushroom elements expressed in (4) [13]. The direction of the electric field of the incident plane wave is assumed to be parallel to the Y-axis.

$$L = \mu t. \quad (2)$$

$$g_y = (\Delta y - W_y). \quad (3)$$

$$C = \frac{\epsilon_0(1+\epsilon_r)W_x}{\pi} \operatorname{arccosh}\left(\frac{\Delta y}{g_y}\right). \quad (4)$$

$$Z_s = j\omega L / (1 - \omega^2 LC). \quad (5)$$

$$\Gamma = (Z_s - \eta) / (Z_s + \eta) = |\Gamma| \exp(j\phi). \quad (6)$$

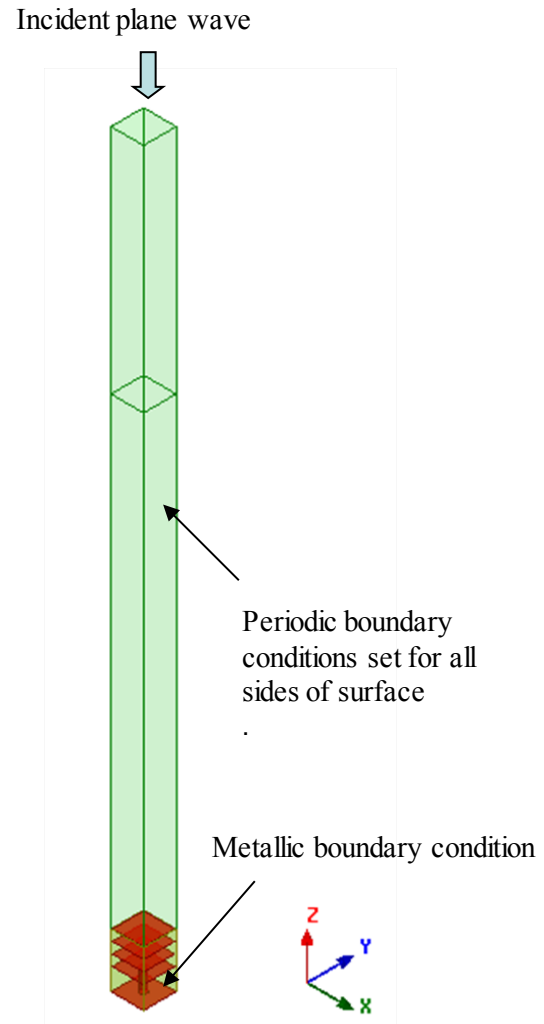
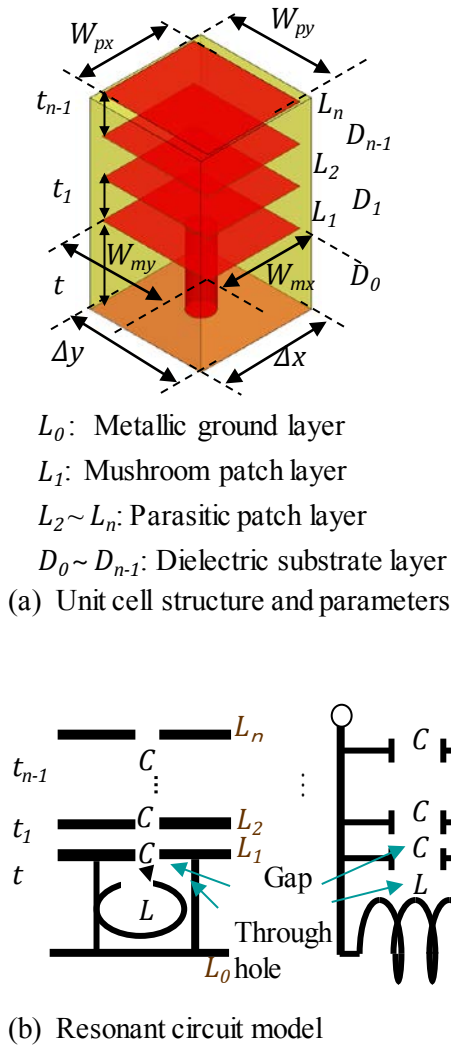


Fig. 1. Multi-layer mushroom structure with parasitic element layers.

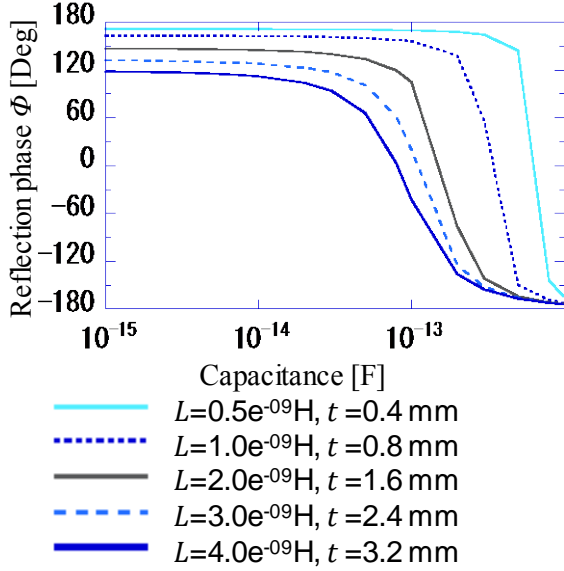


Fig. 2. Relationship between reflection phase  $\phi$  and capacitance  $C$  when inductance  $L$  is a parameter.

The surface impedance of this array,  $Z_s$ , is expressed as (5). The reflection coefficient  $\Gamma$  and reflection phase  $\Phi$  are shown in (6). In (6),  $\eta$  is equal to the impedance in free space. Figure 2 shows the theoretical calculation results using the above formulas of the relationship between reflection phase  $\phi$  and  $C$  when  $L$  is a parameter. The frequency is set to 8.8 GHz, and the mushroom spacings,  $\Delta x$  and  $\Delta y$ , are set to 2.4 mm. When  $L$  is small and  $t$  is thin, the reflection phase range is wide at a high capacitance value and varies rapidly with the variation in the capacitance value.

Next, we describe the multi-layer mushroom structure. When the size of the parasitic patch,  $W_{px}$  (or  $W_{py}$ ), is set to the same size as that of the mushroom patch,  $W_{mx}$  (or  $W_{my}$ ), and both the gap between mushroom patches,  $g_y$ , and that between parasitic patches,  $g_{yp}$ , are the same, the multilayer mushroom structure shown in Fig. 1(a) is regarded to have the capacitance of  $n$ , set parallel in an equivalent circuit model. Therefore, the total capacitance is approximated as  $n$  by  $C$ . The surface impedance of this array is introduced in (7) by changing capacitance “ $C$ ” of (5) to  $n$  times the capacitance, “ $nC$ .”

$$Z_s = j\omega L / (1 - \omega^2 L n C). \quad (7)$$

In the paper, we call the calculation using (1)-(7) as “LC resonant model”.

According to [16, 17], surface impedance is introduced using the other analysis model. We call the model “Theory II” and briefly introduced as follows. In the Theory II, TM- and TE-impedance are shown as (8) and (9), respectively, where  $\theta$  is the angle of incidence and  $\theta_2$  is expressed as formula (10).

$$Z^{TM} = \frac{j\omega\mu \frac{\tan(\beta t)}{\beta} \cos^2(\theta_2)}{1 - 2k_{eff} a \frac{\tan(\beta t)}{\beta} \cos^2(\theta_2)}. \quad (8)$$

$$Z^{TE} = \frac{j\omega\mu \frac{\tan(\beta t)}{\beta}}{1 - 2k_{eff} a \frac{\tan(\beta t)}{\beta} \left(1 - \frac{2}{\epsilon_r + 1}\right) \sin^2(\theta)}. \quad (9)$$

$$\theta_2 = \arcsin\left(\frac{\sin(\theta)}{\sqrt{\epsilon_r}}\right). \quad (10)$$

This paper set  $\theta$  equal to 0 when we calculate reflection phase and then equation (8) and equation (9) are the same. In formula (9),  $k_{eff}$  is the wave number of the incident wave vector in the effective host medium [17].  $\epsilon_{eff}$  is the effective relative permittivity shown as (12) [16]. In formula (8),(9)  $a$  is expressed as equation (13)[17].

$$k_{eff} = k_0 \sqrt{\epsilon_{eff}}. \quad (11)$$

$$\epsilon_{eff} = \frac{\epsilon_r + 1}{2}. \quad (12)$$

$$a = \frac{k_{eff} \Delta y}{\pi} \ln\left(\frac{1}{\sin\frac{\pi g_y}{2\Delta y}}\right). \quad (13)$$

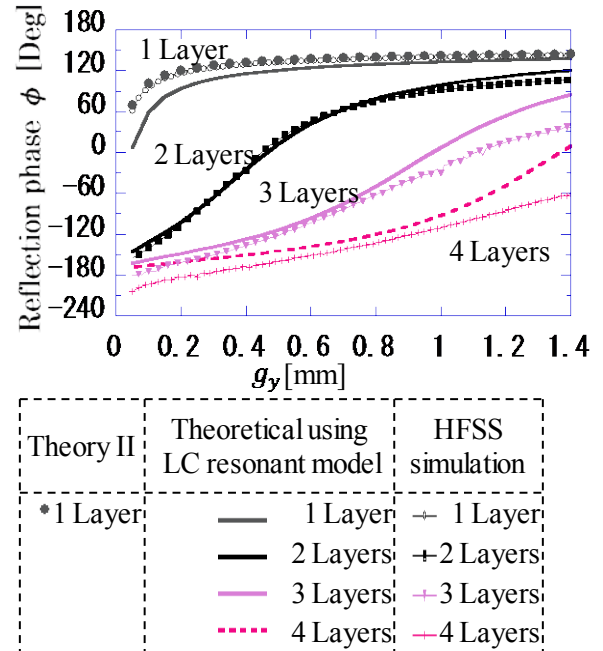


Fig. 3. Reflection phase vs. gap  $g_y$  when number of layers is a parameter.

Figure 3 shows the reflection phase versus the gap size  $g_y$  at 8.8 GHz for a mushroom structure comprising 1 to 4 layers. In this paper, we use HFSS for the simulation because it is popular for the mushroom structure analysis. HFSS is commercial software based on the finite element method (FEM) and uses the weighted residual method. In the HFSS simulation, we use the first order tangential element basis function. An incident plane wave is assumed coming from the Z-axis positive direction to the reflectarray as shown in Fig. 1(c). The electric field vector of the incident plane wave is set parallel to the Y-axis. We use periodic boundary conditions for the side surface of the element cell and the perfect electric conductor (PEC) boundary condition for the ground plane. The periodic spacing of the mushroom structure,  $\Delta x$  and  $\Delta y$ , are given as 2.4 mm. The thickness of the mushroom structure,  $t$ , is set equal to 1.6 mm and the parasitic patch intervals  $t_1, \dots, t_3$  are set equal to 0.8 mm. The relative permittivity of the dielectric substrate,  $\epsilon_r$ , is 4.4. In Figs. 3, 4, and 5, the solid lines represent the theoretical results using LC resonant model from (1)-(7) and the symbols represent the simulation results using the finite element method.

In Fig. 3, the theoretical results using Theory II from (8)-(13) are represented by gray solid circles for 1 Layer. The Theory II results pretty well match the FEM simulated result at 1 Layer. Although theoretical results using the LC resonant model and simulated results do not completely match and the difference increases when gap size  $g_y$  is larger than 1 mm and as the number of layers increases, the graph curves of the theoretical and simulated results have a similar tendency for each of the 1 to 4 layers. Therefore, we can confirm that the proposed approximation shown in (7) is useful in considering qualitatively the role of parasitic layers in a multi-layer mushroom structure and in investigating the physical phenomenon based on theory. We can control the capacitance value by changing the number of parasitic layers. Figure 3 also shows that when we increase the number of parasitic patch layers, we can reduce the reflection phase gradient versus the gap size. This is useful for a highly accurate design. The variation range of the reflection phase when we use parasitic layers is also wider than the case for a non-parasitic layer.

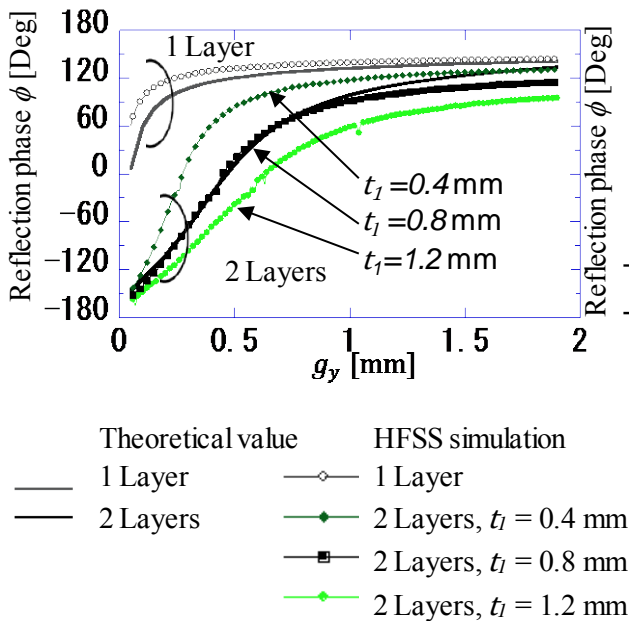


Fig. 4. Reflection phase  $\phi$  vs. gap  $g_y$  of one parasitic layer mushroom (2 Layers) and without parasitic layer (1 Layer) when distance  $t_1$  between parasitic patch and mushroom patch is a parameter.

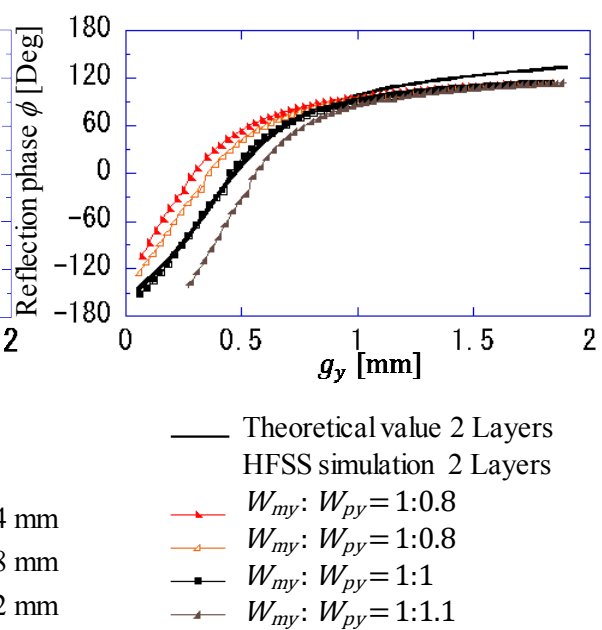


Fig. 5. Reflection phase  $\phi$  vs. gap  $g_y$  for one parasitic layer (2 Layers) when parasitic patch size  $W_{py}$  is a parameter.

Next, we investigate the characteristics of the parasitic patch given by the parasitic size “ $W_{py}$ ” and distance  $t_1$  between the parasitic patches and mushroom patches. Figure 4 shows the reflection phase  $\phi$  versus  $g_y$  of one parasitic layer mushroom (2 layers) and without a parasitic layer (1 layer) when distance  $t_1$  between the parasitic patch and mushroom patch is a parameter. We consider that the proposed multi-layer mushroom structure using parasitic layers has two kinds of capacitance. One capacitance “ $C$ ” exists in gaps between patches, and the other capacitance “ $C_L$ ” exists between layers. In Fig. 4, when interval “ $e$   $t_1$ ” between layers is small, e.g., 0.4 mm, “ $C_L$ ” is considered to be large and it prevents the effect of the parallel arrangement of capacitance  $C$  to increase the value of the capacitance. We adopt 0.8 mm for the value of  $t_1$  in the paper because the difference between the theoretical results using the above formula and the simulated results using the HFSS is minimum. When we use different size patches the capacitance value also changes. Figure 5 shows reflection phase  $\phi$  versus  $g_y$  for one parasitic layer mushroom patch (2 layer mushroom patches) when parasitic patch size  $W_{py}$  is a parameter. The conventional reflectarray using a microstrip patch generally uses a smaller size parasitic patch than the microstrip patch to achieve a broadband reflectarray [14]. In the case of the proposed multi-layer mushroom patches using parasitic patches, when we set mushroom patch size  $W_{my}$  and parasitic patch size  $W_{py}$  to the same value, i.e.,  $W_{my}:W_{py} = 1:1$ , the reflection phase range is wider than when we set  $W_{my}:W_{py} = 1:0.8$  or  $1:0.9$  as shown in Fig. 5. This is because the effect of the parallel arrangement in this structure to achieve a higher capacitance is weakened by using small patches that enlarge the gap between the patches and reduce the capacitance of each gap. On the other hand, when we set  $W_{my}:W_{py} = 1:1.1$ , the  $C$  yield in the gap between parasitic patches can be large. However, when we adopt a larger parasitic patch than the mushroom patch, the adjacent parasitic patches touch each other. Consequently, when we choose the same size for each mushroom patch and parasitic patch, we can gain an advantage by setting the capacitances parallel to obtain a high capacitance and to increase the reflection phase range. The reflection phase versus the frequency

for one parasitic layer (2 layers) and without a parasitic layer (1 layer) is shown in Fig. 6. In 2 layers, both the theoretical results and HFSS calculation results of the reflection phase versus frequency exhibit similar curves and we confirm that the proposed approximation is effective for frequency dependency. A comparison of the 1-layer and 2-layer mushroom structures shows that the resonant frequency that satisfies the reflection phase equal to zero shifts to a lower frequency by using a parasitic patch. From (1) and (2) above, it is considered that the resonant frequency shifts lower due to the increase in the capacitance value. This is because inductance  $L$  is the same for both cases with and without the mushroom structure. The largest difference in the reflection phase between the minimum ( $W_y = 1.187$  mm) and maximum ( $W_y = 2.3$  mm) patches is 183 deg. at 11 GHz for the 1 layer mushroom structure and 240 deg. at 9 GHz for the 2 layer mushroom structure. Therefore, the maximum difference in the reflection phase can be expanded using parasitic elements. When the difference in the reflection phase between adjacent patches,  $\Delta\phi_{k,k+1}$ , shown in (14) satisfies (15) for each  $k$ , a wave is reflected toward control angle  $\alpha$ . The model in Fig. 7 shows when the incident electric field direction and beam control direction are orthogonal.

$$\Delta\phi_{k,k+1} = \phi_k - \phi_{k+1}. \quad (14)$$

$$\alpha = \arcsin(\lambda\Delta\phi/2\pi\Delta y). \quad (15)$$

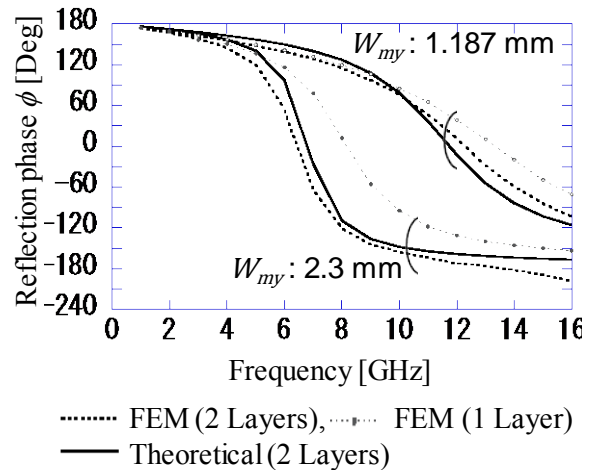


Fig. 6. Reflection phase vs. frequency for one parasitic layer (2 Layers) and without parasitic layer (1 Layer) compared to theoretical calculation.

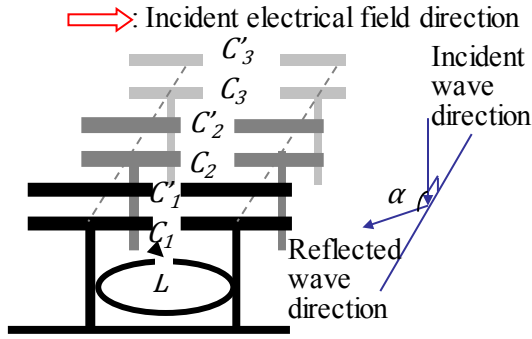


Fig. 7. Design model for multi-layer mushroom structure with parasitic element reflectarray.

### III. DESIGN OF MULTI-LAYER MUSHROOM REFLECTARRAY BASED ON LC RESONANT CIRCUIT THEORY

In this section, we propose a novel design method for a multi-layer mushroom reflectarray with parasitic elements that focuses on the function of  $L$  and  $C$  when the incident electric field direction and beam control direction are parallel. We adopt two-layer patches for a multi-layer mushroom reflectarray, which achieves a wide reflection phase range as in Fig. 3. In the conventional reflectarray design method such as the microstrip reflectarray [12] in which the element sizes are usually almost half the wavelength, the resonant frequency and reflection phase are usually decided by the element size. Therefore, to achieve the desired reflection-phase difference, we usually set different size patch elements ( $W_{my1}, W_{my2}, \dots$ ) at equal distances. Figure 8 shows the conventional reflectarray design model using the patch element length and we call this model the ‘element model.’ Figure 8(a) shows the model when the incident electric field and beam control direction of the scattered waves are set parallel. Figure 8(b) shows the model when the incident electric field and beam control direction of the scattered wave are set orthogonal.

In the conventional method [3,8,12], different size patches are arranged in the reflect beam direction as shown in Fig. 8. In Fig. 8(a), the beam control direction and incident electrical field direction are set parallel to the  $Y$ -axis. Different size patches selected to satisfy the desired reflection phase are arranged along the  $Y$ -axis.

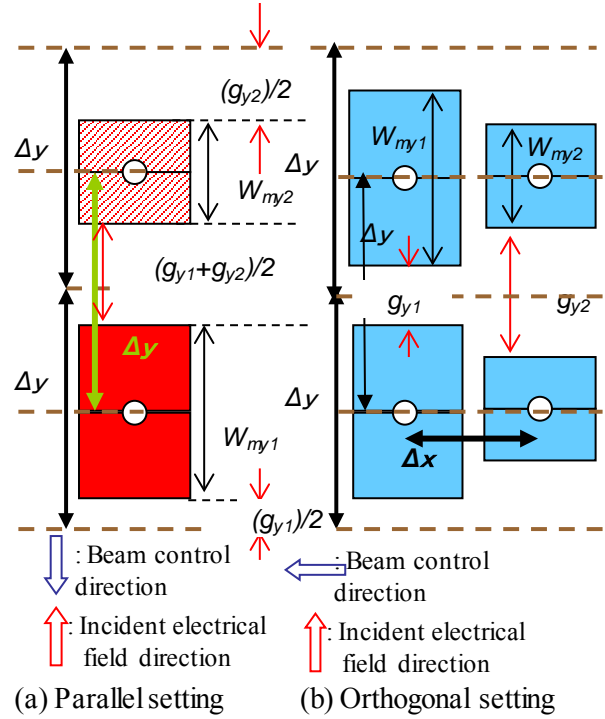


Fig. 8. Conventional element model reflectarray.

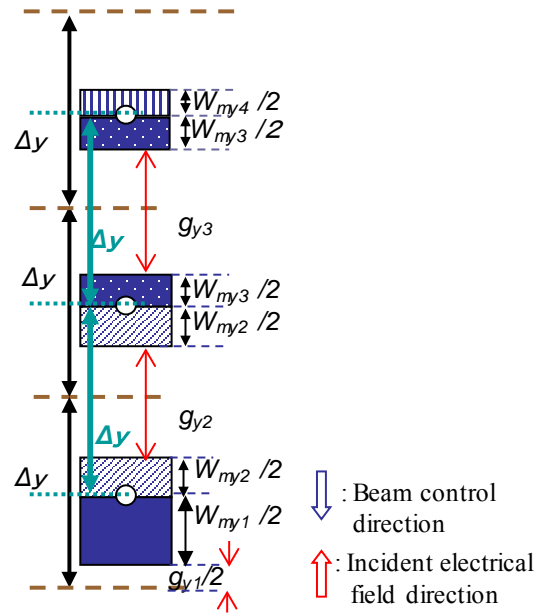


Fig. 9. Proposed gap model reflectarray.

In Fig. 8(b), the beam control direction and incident electrical field direction are set orthogonal. Different size patches selected to satisfy the desired reflection phase are arranged along the  $X$ -axis. However, in the case of Fig. 8(a), the beam control direction and incident

electrical field direction are set parallel, when we set different size patch element ' $W_{y_i}$ ' at equal distances, the gap value is changed from ' $g_{y_i}$ ' to ' $g_{y_i} + g_{y_{i+1}}/2$ '. Nevertheless, in the case of orthogonal beam control as shown in Fig. 8(b), when we set a different size patch element ' $W_{y_i}$ ' at equal distances, gaps ' $g_{y_i}$ ' are also set in the same way. In the case of the mushroom structure, the element sizes are very small and we consider that the resonance is decided by  $LC$  resonance as described in Section II. Therefore, the capacitance value, which is determined by the gap size, is more important than that determined by the element size. To achieve a gap based design, this paper proposes a new design model in which the incident electric field and beam control direction of the scattered wave are set parallel. The model is called the "gap model" and is shown in Fig. 9. In the proposed model, in the first step, we set the via holes to be equally spaced,  $\Delta y$ . In the next step, different size gaps,  $g_{y_i}$ , are chosen that are decided based on the reflection phase shown in Fig. 3. Next, the gaps are allocated so that the center of each gap is also equally-spaced between vias as shown in Fig. 9. Then, half length patches,  $W_{y_i}/2$ , are set on both sides of the gaps. Consequently, the size of each patch is  $(W_{y_i} + W_{y_{i+1}})/2$  as shown in Fig. 9. Please note, in this model, the via hole is not set in the center of the patch. Finally, we can allocate different capacitances at equal spacing using the proposed method because the capacitance value is decided by the gap size as described in Section II.

#### IV. ANALYSIS AND MEASUREMENT RESULTS FOR MULTI-LAYER MUSHROOM REFLECTARRAY

Using the gap-model reflectarray design method that is described in Section III, a 70 deg. beam control mushroom reflectarray with parasitic elements for normal incidence (PV70Gs) can be achieved when the incident electric field and beam control direction of the scattered waves are set parallel. A 2-layer model that has the widest reflection phase range in Fig. 3 is adopted. We use the same frequency and periodic spacing for the mushroom structure,  $\Delta x$  and  $\Delta y$ , as that for the reflection phase calculation shown in Fig. 3, i.e., 8.8 GHz and 2.4 mm, respectively. In order to

achieve a scattering reflect wave beam control angle,  $\alpha$ , which is equal to 70 deg., each mushroom should satisfy the condition where the reflection phase difference,  $\Delta\varphi_{k,k+1}$ , between adjacent mushroom patches is 24 deg. based on (9). The design conditions and parameters of the gap model and element model are given in Table 2. Using the 24 deg. phase difference, 15 gaps are required to cover a 360 deg. reflection phase region. From Fig. 3, we can choose an adequate gap size for each required gap in the gap model. However, from Fig. 3, we can see that a gap smaller than 0.1 mm is necessary to achieve less than -140 deg.; however, it is difficult to achieve this in the fabrication process with high accuracy. We can also see from Fig. 3 that no patches exist in relation to a reflection phase greater than 125 deg. We can prepare 11 gap (12 patches correspond to the gaps) sizes from #1 to #11 that can yield the same phase difference between adjacent arrays and the gap sizes from #12 to #15 are not available as indicated in Table 2.

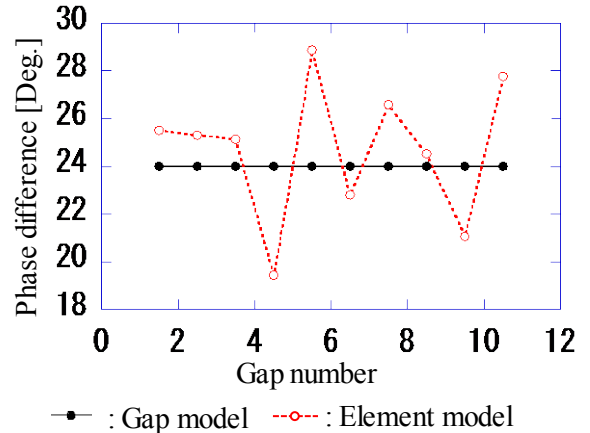


Fig. 10. Reflection phase difference vs. gap number for gap and element models.

In the case of the element model, we primarily decide the element patch size to obtain the required reflection phase that is described in Section III. Then, the reflection phases of the element model shown in Table 2 are decided by the gap size using Fig. 3. The reflection phase difference versus the gap number is shown in Fig. 10. The phase difference in the gap model is maintained at a constant 24 deg.; however, in the element model, the value differs in the range of 10 deg. The gap model and element model

Table 2: Design parameters of PV70Gs

Gap number	Gap model				Element model			
	Symbol	Gap [mm]	Reflection phase [Deg.]	Phase difference [Deg.]	Symbol	Gap [mm]	Reflection phase [Deg.]	Phase difference [Deg.]
#1	$g_{y_1}$	0.1	-139	24	$\frac{g_{y_1}+g_{y_2}}{2}$	0.139	-127	21
#2	$g_{y_2}$	0.177	-115	24	$\frac{g_{y_2}+g_{y_3}}{2}$	0.208	-106	24
#3	$g_{y_3}$	0.238	-91	24	$\frac{g_{y_3}+g_{y_4}}{2}$	0.266	-82	27
#4	$g_{y_4}$	0.294	-67	24	$\frac{g_{y_4}+g_{y_5}}{2}$	0.321	-55	23
#5	$g_{y_5}$	0.348	-43	24	$\frac{g_{y_5}+g_{y_6}}{2}$	0.385	-32	28
#6	$g_{y_6}$	0.422	-19	24	$\frac{g_{y_6}+g_{y_7}}{2}$	0.441	-4	20
#7	$g_{y_7}$	0.46	5	24	$\frac{g_{y_7}+g_{y_8}}{2}$	0.496	16	25
#8	$g_{y_8}$	0.532	29	24	$\frac{g_{y_8}+g_{y_9}}{2}$	0.584	41	25
#9	$g_{y_9}$	0.636	53	24	$\frac{g_{y_9}+g_{y_{10}}}{2}$	0.722	66	25
#10	$g_{y_{10}}$	0.809	77	24	$\frac{g_{y_{10}}+g_{y_{11}}}{2}$	-	91	-
#11	$g_{y_{11}}$	1.213	101	24	-	-	-	-
#12	$g_{y_{12}}$	-	125	-	-	-	-	-
#13	$g_{y_{13}}$	-	149	-	-	-	-	-
#14	$g_{y_{14}}$	-	173	-	-	-	-	-
#15	$g_{y_{15}}$	-	197	-	-	-	-	-
Name					Symbol		Value	
Substrate name					$FR4$		-	
Relative permittivity					$\epsilon_r$		4.4	
Dielectric loss-tangent					$\tan \delta$		0.018	
Via hole diameter					$vd$		0.50 mm $\phi$	
Mushroom height					$t$		1.6 mm	
Interval between parasitic patches					$t_1$		0.8 mm	
Element space of mushroom structure					$\Delta x, \Delta y$		2.4 mm	
Gap size between mushroom patches at x-axis direction					$g_x$		0.1 mm	

reflectarrays are designed using parameters from Table 2.

The HFSS analysis model of the reflectarray (PV70Gs) is shown in Fig. 11. The reflectarray is constructed using a mushroom layer and patch layer. In Fig. 11, the perfect matched layer (PML) boundary condition is used at the top and bottom boundary surfaces and periodic boundary conditions are used at the side boundary surfaces. A plane wave incident along the Z-axis is assumed.

No patch is set if the optimum size patch that satisfies the desired reflection phase does not exist. The metallic ground plane, which represents the unavailability of a desired patch, is also removed to avoid undesired radiation from the ground plane. A mushroom structure usually uses a much smaller mesh for HFSS calculation than the wavelength. Therefore, it is difficult to analyze a large-scale mushroom array. This paper uses array factor approximation using the basic analysis

model shown in Fig. 11 and the periodic boundary conditions.

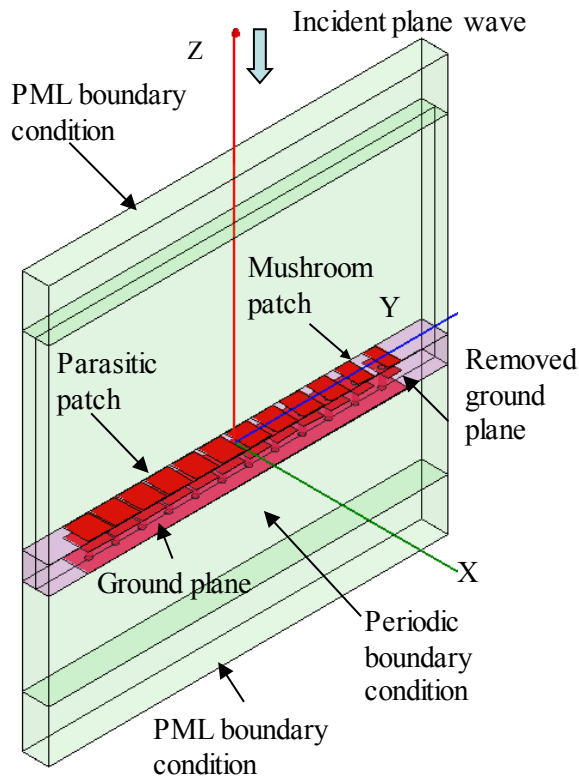


Fig. 11. The analysis model of 70 degree vertical beam control reflectarray (gap model); PV70Gs.

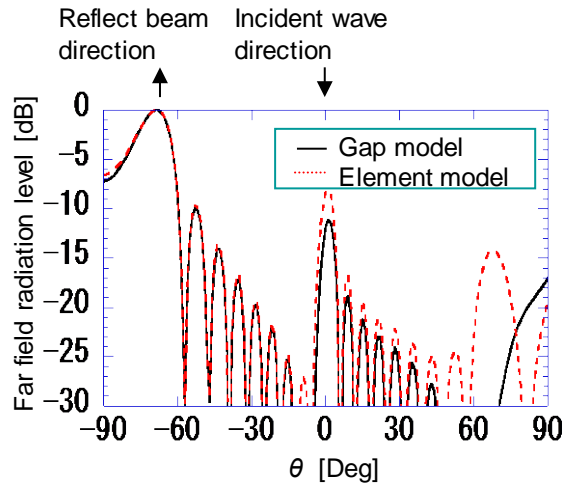
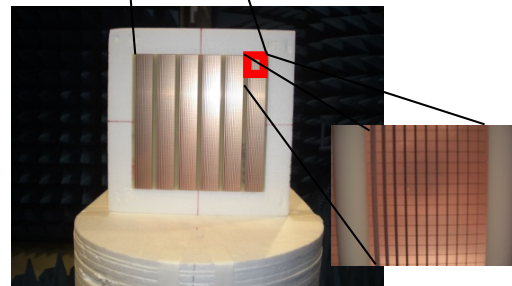
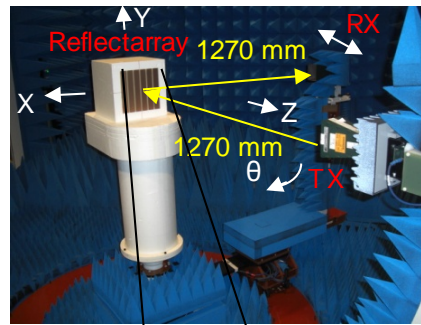


Fig. 12. Far field patterns for element and gap models (calculation results).

The far field scattering patterns of the gap model and element model reflectarrays are shown in Fig. 12. In Fig. 12, we arrange 129 arrays in the X-axis direction and 9 arrays in the Y-axis

direction using an array factor and construct a 310 mm by 325 mm reflectarray. The levels are normalized to the peak level in the  $-70$  deg. direction. Both results using the gap model and element model have a peak level at the desired  $-70$  deg. and a radiation level in undesired directions, i.e., imaging direction ( $\theta = 0^\circ$ ) and  $70$  deg. direction of the conventional element model are higher than those for the proposed gap model. From Figs. 11 and 12, we can confirm that the proposed gap model is superior to the conventional element model.



Parasitic layer surface

Fig. 13. Measurement system and multi-layer mushroom reflectarray with parasitic element designed using gap model (217 mm  $\times$  217 mm).

Next, we fabricate a 217 mm by 217 mm gap model reflectarray and measure the scattering of reflected and transmission waves in the chamber. Photographs of the measurement system and reflectarray are shown in Fig. 13. In the system, the reflectarray is set at the center and the distances between the reflectarray and transmitter antenna (TX) and that between the reflectarray and receiver antenna (RX) are set to 1270 mm. The TX is set in front of the reflectarray and an incident wave is assumed from  $\theta = 0^\circ$  direction (The coordinate system is shown in Fig. 13). The RX

horn is moved on a rail along the circumference of a circle to scan the scattering level.

Generally, the measurement distance must satisfy (16) for a radar cross-section measurement [18]. In (16), “ $D$ ” represents the maximum diameter of the target, which we set to 217 mm. Therefore, the measurement distance must be longer than 2500 mm. However, it is difficult to maintain a dynamic range when we use a long measurement distance or a small reflectarray. Moreover, the chamber size is limited.

$$\rho > \frac{2D^2}{\lambda}. \quad (16)$$

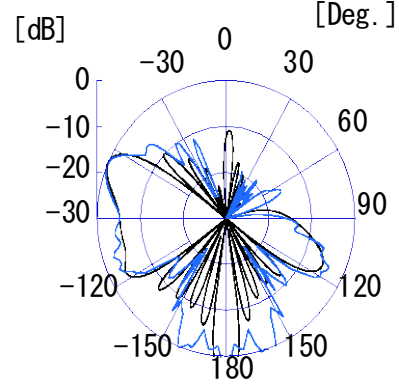
The far field scattering pattern of the measurement and calculated results are shown in Fig. 14. To avoid collision between the TX and RX, the measurement range is set to  $20^\circ < \theta < 340^\circ$ . In the  $-20^\circ < \theta < 20^\circ$  region, only simulated results are shown in the graph. In Fig. 14(a), the levels are normalized to 0 dB at the peak level at -70 deg. Figure 14(b) shows the actual measured value in the chamber using the settings indicated in Fig. 13 by the aqua colored line. In the measurement, we set the level equal to 0 dB when the transmission cable and received cable are directly connected. We use standard horn antennas (Flan Microwave LTD.) and the directivity gain at the 8.8 GHz is 18.6 dBi. The black line in Fig. 14(b) shows the theoretically calculated received level using the radar equation (17) and radar cross section  $\sigma_r$  of the reflectarray calculated using HFSS.

$$W_a(\theta, \varphi) = \frac{\lambda^2 G_a^2}{(4\pi)^3 R^4} W_t \sigma_r(\theta, \varphi). \quad (17)$$

The symbol name and value used in (17) are shown in Table 3.

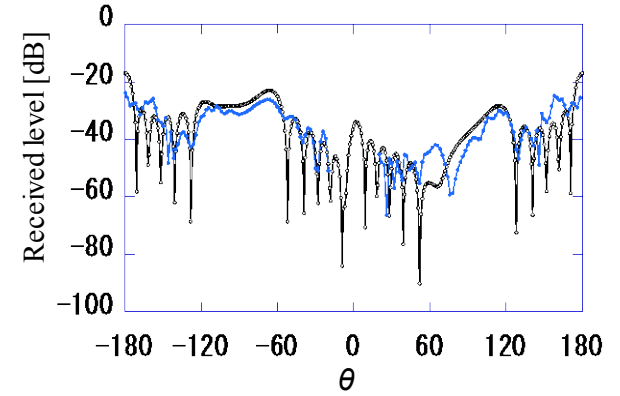
Table 3: Symbol name and value used in radar equation

Name	Symbol	Value
Received power	$W_a$	
Transmission power	$W_t$	1 mW
Antenna gain; standard horn from Flan micro	$G_a$	18.6 dBi
Distance between transmission antenna and reflectarray	$R$	1270 mm
Radar cross section of reflectarray	$\sigma_r$	Calculated using HFSS
Wavelength (8.8 GHz)	$\lambda$	0.034



- Normalized simulation result ( $0^\circ \leq \theta \leq 360^\circ$ )
- Normalized measurement result ( $20^\circ \leq \theta \leq 340^\circ$ )

(a) Far field scattering pattern (normalized).



- Theoretical result using radar cross section (RCS) calculated by HFSS and radar equation.
- Actual measured value in chamber

(b) Actual measurement value and theoretical result from radar equation and simulated RCS.

Fig. 14. Comparison between theoretical, simulated, and measurement results of far field scattering pattern.

In Fig. 14(b), the values in the desired  $-70$  direction are  $-26.3$  dB<sub>m</sub> (measurement) and  $-23.4$  dB<sub>m</sub> (theoretical). The difference is 2.9 dB. There exists a side lobe level at  $\theta$  equal to  $70$  deg. that is in the opposite axial direction of the desired  $-70$  deg. Because we use the element spacing of 2.4 mm and 15 divisions for one period in the  $-70$  deg. reflection beam direction, in the design of the  $70$  deg. beam control we also use the same element spacing of 2.4 mm and 15 divisions. The

design differences in the reflected beam control between 70 deg. and  $-70$  deg. are represented by the phase difference between adjacent elements of  $-24$  deg. or 24 deg. Therefore, when the difference in the reflection phase between adjacent elements is shifted due to manufacturing error, the side lobe level is increased. In Fig. 14, there also exists a side lobe level at " $\theta$ " equal to the direction caused by specular reflection in the simulation. Please note that the direction cannot be measured. Under the conditions given above for array factor approximation analysis and measurement in a small chamber, we confirm that the graphs of the calculation and measurement scattering radiation pattern results are overlapped except for the back lobe radiation. In the reflectarray design of the paper, we assume the incident wave is coming from the upper side (" $\theta$ " equal to 0 deg. direction). However, when we use the reflectarray to improve the propagation environment, the waves come from several oblique directions [3, 20]. Otherwise, the mushroom like structure exhibits dual resonant behavior for an oblique incident as reported in [16 and 19]. We need further study for these oblique incidents for the reflectarray.

## V. CONCLUSION

This paper proposed a novel reflectarray design using a multi-layer mushroom structure with parasitic elements based on capacitance value control in the  $LC$  resonant circuit model. Based on the study of the  $LC$  resonant circuit model, this paper showed that the parallel set capacitance value can be theoretically controlled using the number of parasitic layers. This paper also proposed a novel reflectarray design method for a 70 deg. beam control mushroom reflectarray when the incident electric field and beam control direction of the scattered waves are set parallel by focusing on the capacitance value. Finally, this paper showed that the proposed design exhibits good performance by comparing the simulated and experimental results.

## ACKNOWLEDGMENT

This work was carried out by "the research and development project for expansion of radio spectrum resources" from The Ministry of Internal Affairs and Communications, Japan. The authors especially thank Prof. Shinji Uebayashi of Chukyo

University, Prof. Kunio Sawaya of Tohoku University, and Dr. Long Li and Dr. Atsushi Murase of NTT DOCOMO who provided continuous support for this study.

## REFERENCES

- [1] R. Fisher, "60 GHz WPAN Standardization within IEEE 802.15.3c," *Signals, Systems and Electronics*, 2007. ISSSE '07, pp. 103 - 105, 2007.
- [2] L. Li, Q. Chen, Q. Yuan, K. Sawaya, T. Maruyama, T. Furuno, and S. Uebayashi, "Microstrip Reflectarray using Crossed-Dipole with Frequency Selective Surface of Loops," *ISAP2008*, TP-C05, 1645278, 2008.
- [3] T. Maruyama, T. Furuno, and S. Uebayashi, "Experiment and Analysis of Reflect Beam Direction Control Using a Reflector Having Periodic Tapered Mushroom-Like Structure," *ISAP2008*, MO-IS1, 1644929, p. 9, 2008.
- [4] L. Li, Q. Chen, Q. Yuan, K. Sawaya, T. Maruyama, T. Furuno, and S. Uebayashi, "Frequency Selective Reflectarray using Crossed-Dipole Elements with Square Loops for Wireless Communication Applications," *IEEE Trans. Antennas Propagat.*, vol. AP-59, no. 1, pp. 89-99, 2011.
- [5] L. Li, Q. Chen, Q. Yuan, K. Sawaya, T. Maruyama, T. Furuno, and S. Uebayashi, "Novel Broadband Planar Reflectarray with Parasitic Dipoles for Wireless Communication Applications," *IEEE APWL*, vol. 8, pp. 881-885, 2009.
- [6] T. Maruyama, T. Furuno, T. Ohya, Y. Oda, Q. Chen, and K. Sawaya, "Dual Frequency Selective Reflectarray for Propagation Improvement," *IEEE iWAT*, 2010, pp. 1-4, 5464764, March 2010.
- [7] D. Sievenpiper, J. H. Schaffner, H. J. Song, R. Y. Loo, and G. Tansonan, "Two-Dimensional Beam Steering using an Electrically Tunable Impedance Surface," *IEEE Trans. Antennas Propagat.*, vol. AP-51, no. 10, pp. 2713-2722, Oct. 2003.
- [8] K. Chang, J. Ahn, and Y. J. Yoon, "Artificial Surface Having Frequency Dependent Reflection Angle," *ISAP 2008*.
- [9] K. Chang, J. Ahn, and Y. J. Yoon, "High-Impedance Surface with Nonidentical Lattices," *IEEE iWAT 2008*, P315, pp. 474-477, 2008.
- [10] F. Yang and Y. Rahmat-Samii, "Polarization Dependent Electromagnetic Band Gap (PDEBG) Structure: Design and Applications," *Microwave Opt. Technol. Lett.*, vol. 41, no. 6 pp. 439-444, July 2004.
- [11] D. Sievenpiper, L. Zhang, R. F. J. Broas, N. G. Alexopolous, and E. Yablonovitch, "High-Impedance Electromagnetic Surfaces with a

- Forbidden Frequency Band,” *IEEE Trans. Microwave Theory and Techniques* vol. MTT-47, no. 11, pp. 2059-2074, Nov. 1999.
- [12] D. M. Pozar, T. S. Targonsky, and H. D. Syrigos, “Design of Millimeter Wave Microstrip Reflectarrays,” *IEEE Trans. Antennas Propagat.*, vol. AP-45, no. 2, pp. 287-295, 1997.
- [13] D. F. Sievenpiper, “High-Impedance Electromagnetic Surfaces,” Ph.D. Dissertation, UCLA, 1999.
- [14] J. Huang, *Reflectarray Antennas*, IEEE Press, Wiley-Interscience, pp. 97-99, 2007.
- [15] A. B. Yakovlev, M. G. Silveirinha, O. Luukkonen, C. R. Simovski, I. S. Nefedov, and S. A. Tretyakov, “Characterization of Surface-Wave and Leaky-Wave Propagation on Wire-Medium Slabs and Mushroom Structures Based on Local and Non-Local Homogenization Models,” *IEEE Trans. Microwave Theory and Techniques*, vol. MTT-51, no. 11, pp. 2700-2714, November 2009.
- [16] O. Luukkonen, M. G. Silveirinha, A. B. Yakovlev, C. R. Simovski, I. S. Nefedov, and S. A. Tretyakov, “Effects of Spatial Dispersion on Reflection from Mushroom-type Artificial Impedance Surfaces,” *IEEE Trans. Microwave Theory and Techniques*, vol. MTT-51, no. 11, pp. 2692-2699, November 2009.
- [17] O. Luukkonen, C. Simovski, G. Granet, G. Goussetis, D. Lioubtchenko, A. V. Raisanen, and S. A. Tretyakov, “Simple and Accurate Analytical Model of Planar Grids and High-Impedance Surfaces Comprising Metal Strips or Patches,” *IEEE Trans. Antennas Propagat.*, vol. 56, no. 6, pp. 1624-1632, 2008.
- [18] W. L. Stutzman and G. A. Thiele: “Antenna Theory and Design,” second edition, Wiley, 1998.
- [19] L. Li, Q. Chen, Q. Yuan, L. Changhong, and K. Sawaya, “Surface-Wave Suppression Band Gap and Plane-Wave Reflection Phase Band of Mushroom Like Photonic Band Gap Structures,” *Journal of Applied Physics*, vol.103, pp. 023513-023513-10, 2008.
- [20] K. Shin, Y. Oda, T. Furuno, T. Maruyama, and T. Ohya, “A Novel Approach for Capacity Improvement of 2x2 MIMO in LOS Channel Using Reflectarray,” *IEEE VTC* 2011 Spring, 2011.

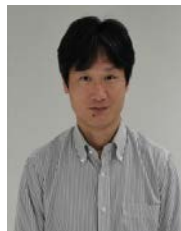


**Tamami Maruyama** is a senior research engineer at the NTT DOCOMO Research Laboratories. She received her B.S. and M.S. degrees in 1985 and 1988, respectively, from the department of mathematics, Tsuda College, Tokyo, Japan. In 2001, she received

her Ph.D. degree from Tohoku University, Sendai, Japan. In 1988, she joined the Nippon Telegraph and Telephone Corporation (NTT). In 2003, she joined NTT DOCOMO INC. In 1995, she received the Young Engineer Award from IEEE AP-S Tokyo Chapter. In 1998, she received the Excellent Paper Award from the IEICE. In 2008, she received the Best Paper Award from ISAP 2008. Dr. Maruyama is a member of the IEEE and IEICE. Her main research interests include the optimum antenna design method, genetic algorithm, application of metamaterials and reflectarray to wireless communications, design of multi-frequency antennas for digital mobile communication base stations, small sector antennas for indoor high-speed wireless LANs and small multi-band antennas that employ the genetic algorithm for handsets.



**Tatsuo Furuno** received the B.S. degree from Niigata University, Japan, in 1986. He joined NTT and engaged in the research and development of cordless telephone system, radio propagation characteristics for PHS (personal handy-phone system) and Wireless LAN. He joined NTT DOCOMO in 1999 and engaged in the research and development of public wireless LAN service, indoor radio propagation and cognitive radio. He is currently a senior research engineer at NTT DOCOMO Research Laboratories.



**Yasuhiro Oda** received the B.S. degree in Physics from Nagoya University, Nagoya, Japan, in 1990. He joined the Nippon Telegraph and Telephone Corporation (NTT) Laboratories, Kanagawa, Japan, in 1990. He has been engaged in research on radio propagation for land mobile communication systems, radio link design, and positioning technologies. Since 1992, he has been with the Research and Development Department, NTT Mobile Communication Network Inc. He is currently an Executive Research Engineer of Research Laboratories, NTT DOCOMO, Inc.



**Jiyun Shen** was born in Shanghai, China. He received his B.S. and M.S. degrees in 2001 and 2003, respectively, from the undergraduate department of Electrical and Electronic Engineering and the graduate department of Communications and Computer Engineering, Kyoto University, Japan. From 2003, he became a research engineer of the NTT

DOCOMO Research Laboratories. In 2008, he received the Young Researcher's Award from the IEICE. His current main research interests include location algorithm, global positioning system (GPS), orthogonal frequency-division multiplexing (OFDM), multiple-input multiple-output (MIMO), channel coding, radio wave propagation analysis, radio wave signal processing. He is a member of IEICE communications society.



**Tomoyuki Ohya** received his B.E. and M.E. degrees in Electronic Engineering from Kyoto University in 1986 and 1988 respectively, and his M.S. degree in Management of Technology from Massachusetts Institute of Technology in 2000. He joined Nippon Telegraph and Telephone Corporation (NTT) in 1989, and since 1992, he has been working at NTT DOCOMO. He was engaged in the research and development of digital signal processing technologies and wireless transmission technologies. He received Young Researcher's Award from IEICE in 1995. He is a member of IEEE, IEICE and The Acoustical Society of Japan.

Currently, he is a general manager of technology & solution department in mmbi, Inc., and in charge of standardization and development of ISDB-Tmm mobile multimedia broadcasting technologies.